

## Article

# Numerical Simulation of Spiral Cutter–Soil Interaction in Deep Vertical Rotary Tillage

Wang Yang, Xiong Xiao, Ronghui Pan, Shengyuan Guo and Jian Yang \*

College of Mechanical Engineering, Guangxi University, Nanning 530004, China

\* Correspondence: gxuyangjian@163.com; Tel.: +86-13557014056

**Abstract:** Deep vertical rotary tillage (DVRT) is a new tillage method which combines the advantages of deep tillage and rotary tillage. However, limited research has been conducted on a critical component of the deep vertical rotary tiller, namely the spiral cutter. In clay loam, there are a lot of large clods in the topsoil layer after tillage, and the cutting resistance and vibration of the cutter are substantial. To reveal the reasons behind this, a simulation model of a spiral cutter–soil system was developed using Smoothed Particle Hydrodynamics (SPH). Using this model, the working process and force of a spiral cutter were thoroughly investigated. The results show that soil fragmentation, swelling, and loosening primarily result from the combined effects of the separation cutting, velocity difference cutting, auxiliary cutting, and the spiral blade’s lifting effect on soil. The reasons for the larger clods are that topsoil furrow slices are larger and the velocity difference cutting is insufficient. The substantial resistance of the cutter is mainly due to the greater resistance of the blade and the bottom edge, and too many blades cutting the soil simultaneously. Furthermore, due to the asymmetry of the cutter’s structure, the resistance’s amplitude reaches 1963.5 N, which causes the cutter’s large vibration. These findings would be an important basis for optimal cutter design.

**Keywords:** deep vertical rotary tillage; spiral cutter–soil interaction; smoothed particle hydrodynamics



**Citation:** Yang, W.; Xiao, X.; Pan, R.; Guo, S.; Yang, J. Numerical Simulation of Spiral Cutter–Soil Interaction in Deep Vertical Rotary Tillage. *Agriculture* **2023**, *13*, 1850. <https://doi.org/10.3390/agriculture13091850>

Academic Editor: Jin He

Received: 12 August 2023

Revised: 18 September 2023

Accepted: 19 September 2023

Published: 21 September 2023



**Copyright:** © 2023 by the authors. Licensee MDPI, Basel, Switzerland. This article is an open access article distributed under the terms and conditions of the Creative Commons Attribution (CC BY) license (<https://creativecommons.org/licenses/by/4.0/>).

## 1. Introduction

In areas with unpredictable rainfall and pronounced drought periods, deep tillage can effectively improve crop yield [1]. Deep vertical rotary tillage (DVRT), a new tillage method which has emerged in China in recent years, combines the advantages of deep tillage and rotary tillage to better reduce soil bulk density and loose soil [2–4]. This approach employs a deep vertical rotary tiller to cut the soil vertically, subsequently breaking, lifting, and loosening the soil. It can break the plough pan without changing the vertical layering of the soil, and its working depth is up to 30–50 cm [2,5]. Currently, this farming method has been applied to a number of crops in China, including cassava, sugarcane, cotton, corn, and potato [2,6].

A tillage device for DVRT has been invented [7]. It is driven by a tractor and can essentially achieve DVRT. Its forward velocity is 0.1–0.2 m·s<sup>−1</sup>, which is slower. Due to the low working efficiency of the first generation of machines, Li (2016) invented a new type of deep vertical rotary tiller [8]. It is a self-propelled deep vertical rotary tiller. Its forward velocity is 0.5–1.1 m·s<sup>−1</sup> and its tillage depth is 30–50 cm. It is suitable for sandy soil and loam, but for clay-loam, there are a lot of larger clods in the topsoil layer after tillage. Moreover, its power consumption and vibration are substantial. For example, in the common dry land (red clay-loam) of Guangxi Province, China, when the tillage depth is 40 cm, the power consumption of unit tillage width is 90–120 kw·m<sup>−1</sup> and the maximum vibration acceleration of the spiral cutter transmission box is 25 m·s<sup>−2</sup>. Liu et al. (2017) invented a new type of spiral cutter. Its lower part is a spiral structure, and its upper part is a knife-roller structure [9]. However, its working effects have not been reported. Li (2015) analyzed the strength problem of the deep vertical rotary tiller’s transmission box and

proposed corrective opinions and measures to improve the strength of the transmission box [10]. The above indicates that the research on the deep vertical rotary tiller is still in its infancy, and the research on spiral cutter–soil interaction is insubstantial. For clay-loam, using the existing spiral cutter for tillage, there are large clods in the topsoil layer, and substantial cutting resistance and vibration of the spiral cutter. Moreover, in DVRT, there is a large degree of deformation and fragmentation of soil, and complex spiral cutter–soil interaction. And when the spiral cutter works in the soil, it is difficult to observe the interaction process between the spiral cutter and the soil via physical testing and to determine the forces acting on the blade and the spiral blade. Therefore, it is necessary to adopt advanced research methods to study the spiral cutter–soil interaction in DVRT, in order to determine the cause of the larger topsoil clods after tillage and the large cutting resistance and vibration of the spiral cutter, which provide a basis for optimization in the design of spiral cutters.

The simulation method can effectively solve scientific problems which are difficult to solved with physical tests. The finite element method (FEM) [11–15] and discrete element method (DEM) [16–20] are the commonly used simulation methods in tillage research now. FEM is a numerical method based on mesh. When a large deformation occurs, mesh distortion is easily generated, which results in the calculations' non-convergence [21]. However, less time is required to solve this issue. DEM has no mesh. It can effectively solve the problem of large deformations. But determining the contact parameters is difficult [22]. Smoothed-particle hydrodynamics (SPH) is a meshless method, and it can effectively simulate large deformations. Furthermore, it is easy to obtain the soil material parameters. Nowadays, SPH has been used for study different tillage tools' interactions with soil [23–31].

The objective of this study was to develop a simulation model for the spiral cutter–soil system using SPH, and then to verify the validity of the modeling approach through field testing. Finally, we investigate the working mechanism and forces acting on the spiral cutter using this model. The results of study will be the basis for the optimal design of the spiral cutter.

## 2. Materials and Methods

### 2.1. Structure and Working Principle of Deep Vertical Rotary Tiller

The deep vertical rotary tiller is mainly composed of chassis, cab, engine, hydraulic lifting device, rotary tillage device, etc., as shown in Figure 1. The rotary tillage device includes hydraulic motor, transmission box, tillage component, etc. The tillage component is a key component in the deep vertical rotary tiller. It consists of a row of paired and reverse-rotating spiral cutters. The spiral cutter consists of a spiral blade, shaft, and blades that are regularly arranged at the edge of the spiral blade. The structural diagram of the tillage component is shown in Figure 2. When the deep vertical rotary tiller is in operation, first, the spiral cutters rotate and move down to the specified tillage depth under the driving of the hydraulic system. Then, the rotary spiral cutter moves forward with the machine and cuts the soil vertically to break, lift, and loosen the soil.

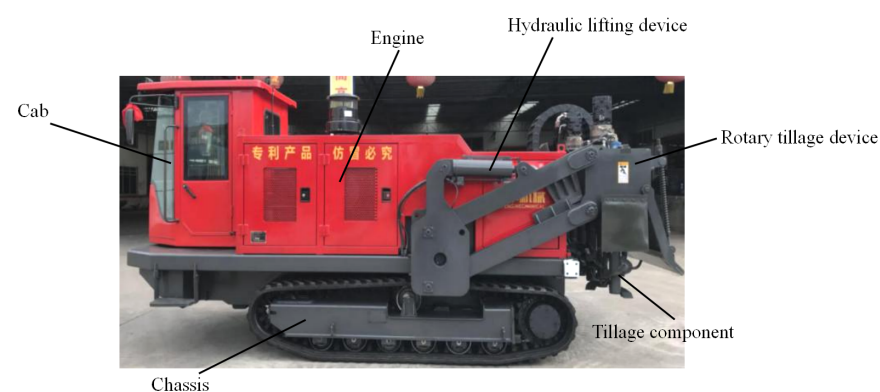


**Figure 1.** Deep vertical rotary tiller.

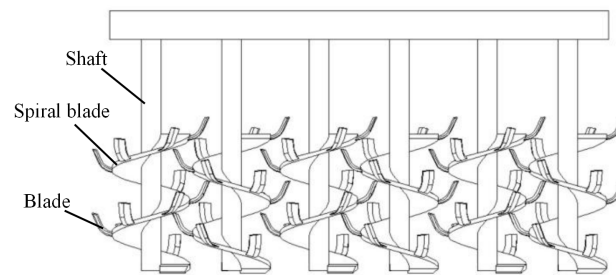


**Figure 2.** Structure diagram of tillage component.

## 2.2. Field Test

### 2.2.1. Test Field

To reduce the influence of impurities such as residual roots on the validation test results, the spiral cutter tillage test was carried out in the field with less impurities and small soil hardness differences. The test field is located in the suburb of Rong County, Yulin City, Guangxi Province, China (lat. 22.85° N, long.110.58° E). The soil is sandy clay loam. The soil mechanical components are shown in Table 1. The measurement method of soil property parameters was the same as that in the literature [13]. The soil property parameters measured are shown in Table 2.

**Table 1.** Soil mechanical component in the verification test.

Soil Particle Size/mm	2–1	1–0.5	0.5–0.25	0.25–0.075	0.075–0.02	0.02–0.002	<0.002
Mass percent (%)	6.66	11.31	15.53	13.48	27.68	8.74	16.60

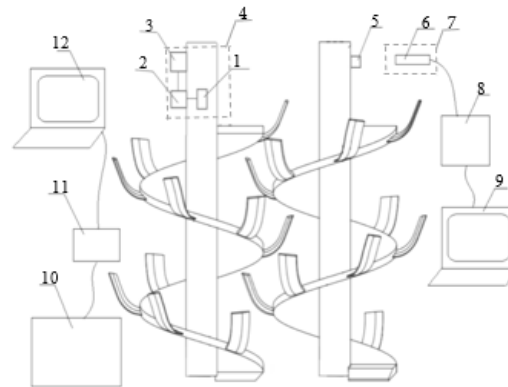
**Table 2.** Soil property parameters in the verification test.

Depth/mm	Bulk Density /g·cm <sup>-3</sup>	Cohesion /Pa	Moisture Content /%	Internal Friction Angle /°	Elasticity Modulus /MPa	Bulk Modulus /MPa	Shear Modulus /MPa
0–100	1.418	4263	21.54	29.85	0.85	0.708	0.327
100–200	1.557	5290	21.72	27.42	1.32	1.1	0.508
200–300	1.593	8527	24.18	32.05	1.83	1.525	0.704
300–400	1.460	7974	32.10	27.24	1.25	1.041	0.481

### 2.2.2. Test Equipment

Main experimental facilities were as follows: self-propelled deep vertical rotary tiller (1SGL-200, Guangxi Wufeng Machinery Co., Ltd., Yulin, China), wireless torque testing system (Donghua DH5905, Donghua Testing Technology Co., Ltd., Jingjiang, China, the sampling rate is up to 4 kHz, the frequency response range is DC~200 Hz ( $\pm 0.1$  dB)@4 kHz sampling frequency, the full degree of strain measurement is  $\pm 53,333 \mu\epsilon$ ,  $\pm 26,667 \mu\epsilon$  and  $\pm 13,333 \mu\epsilon$ , respectively, and the indication error is  $\pm(0.5\% \text{ red} \pm 3 \mu\epsilon)$ ), data acquisition and analysis system (Donghua DH5902, Donghua Testing Technology Co., Ltd., Jingjiang, China), reflective photoelectric sensor (Donghua Testing Technology Co., Ltd., Jingjiang, China), laptop and self-made torque measuring sensor. According to the literature [32], the torque sensor consisted of two special torque test strain gauges BF350-3HA. (The tolerance of resistance to nominal value is  $350 \pm 3 \Omega$ , the deviation of resistance to average value is less than or equal to  $0.4 \Omega$ , and the sensitivity coefficient and dispersion is  $2.1 \pm 1\%$ ). Each special strain gauge includes two strain gauges at an angle of 45 degrees to each other. In the axial direction of the spiral cutter, the special strain gauges were pasted on the positive and anti-symmetric surfaces of the shaft, respectively. The bridge connection of the strain gauges was full bridge connection. The torque sensor was connected to the DH5905 wireless torque test system. The rotational speed sensor included a reflector pasted on the surface of the spiral cutter shaft and a fixed reflective photoelectric sensor, and the

distance between them was 2 cm. The reflective photoelectric sensor was connected with the DH5902 data acquisition system. The sampling frequency of the test systems are both 1 kHz. Two protective devices were installed to protect the sensors and test system from the influence of flying mud. The schematic diagram of the test system is shown in Figure 3. Sensor installation is shown in Figure 4.



1.Torque sensor, 2.Wireless acquisition module, 3.Module power, 4.Protective device, 5.Reflector, 6.Reflective photoelectric sensor, 7.Protective device, 8.Data acquisition system, 9.Laptop, 10.Mobile power, 11. Router, 12.Laptop.

**Figure 3.** Schematic diagram of the test system.



(a) Torque sensor



(b) Speed sensor

**Figure 4.** Sensor Installation.

### 2.2.3. Test Method

Each pair of reverse rotating spiral cutters in the deep vertical rotary tiller plays the same role. To facilitate analysis, only one pair of spiral cutters was retained in the field test, and the rest were removed. In this paper, the torque sensor was used to measure the soil cutting torque of the spiral cutter, and the rotational speed sensor was used to measure the rotational speed of the spiral cutter shaft. The field experiment device is shown in Figure 5. In order to reduce the interference of the test device installed on the spiral cutter shaft to the soil ascending movement, the tillage depth was taken as 30 cm. The length of each test area is 20 m, each end is left 5 m as the transition area, and the remaining middle 10 m is the data acquisition area. The average forward velocity of the spiral cutter was calculated by measuring the time that the deep vertical rotary tiller moved forward in the data acquisition area. The test was repeated 3 times.

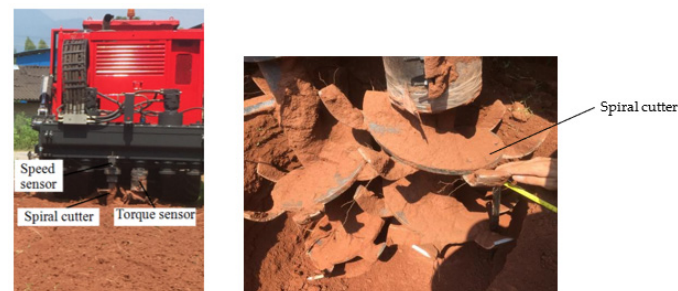


**Figure 5.** Field experiment device.

### 2.3. The Spiral Cutter–Soil System Model

#### 2.3.1. Geometric Model

The modeling size of the spiral cutter was the same as that of the test prototype, but the fastening bolts connecting the blades with spiral blade and the fastening joint part of blades were removed for the convenience of modeling. The main geometric dimensions of the spiral cutters are shown in Figure 6. In addition, the thickness of the spiral blade, the spiral blade bottom edge, the blade and the blade edge was 16 mm, 4 mm, 8 mm, and 2 mm, respectively. The angle of the bottom edge was  $30^\circ$ . The geometrical dimensions of the left and right spiral cutters were the same, but their spiral direction and blade direction were opposite. There were 13 blades on each spiral cutter, and they were evenly fastened on the outer edge of the spiral blade.

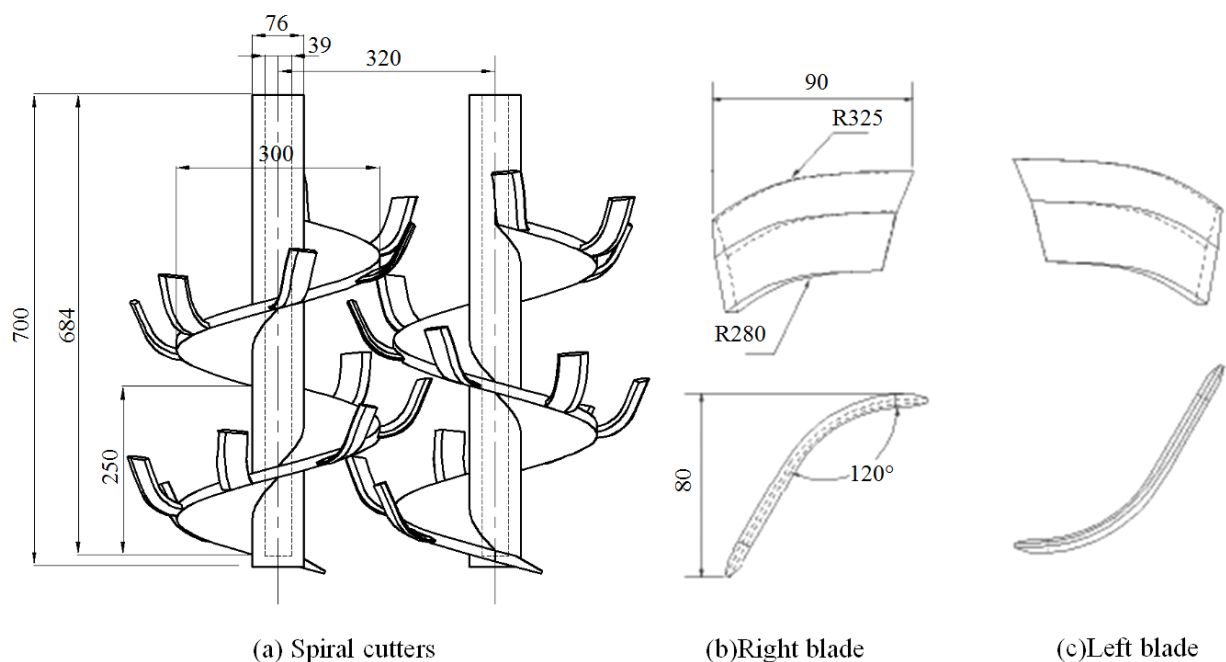


**Figure 6.** Geometric dimensions of spiral cutters.

Due to the changes in physical characteristic parameters as the soil depth changes, in order to accurately simulate the soil conditions at different depths, layered modeling is used for the soil. In this paper, the soil was divided into four layers for modeling, including three layers for tillage layer and one layer for bottom soil. Meanwhile, for meeting the requirements of simulation accuracy and saving calculation time, the width of the soil model should be larger than the working width of the two spiral cutters and the length of the soil model should be appropriate. And in the torque measurement test, the total thickness of the tillage layer was 30 cm. Thus, in order to verify the rationality of the modeling method, the thickness of the model's tillage layer was set as 30 cm, and the thickness of each tillage layer was 10 cm. And the preliminary simulation test showed

that when the bottom soil thickness was greater than 3 cm, the simulation result basically remained unchanged, hence, it was set as 3 cm. Finally, the soil was modeled as a cuboid and the size was determined as 100 cm × 120 cm × 33 cm. The depth of the spiral cutters in the soil was 30 cm.

### 2.3.2. Material Model

The spiral cutter was built as a rigid body. MAT20(MAT\_RIGID) [33] was the material model. The density is  $7.8 \times 10^3 \text{ kg}\cdot\text{m}^{-3}$ . The Poisson's ratio is 0.27 and the elastic modulus is  $2 \times 10^{11} \text{ Pa}$ . The soil's material model was MAT147(MAT\_FHWA\_SOIL) in LS-DYNA [34]. The main parameters of the soil model are shown in Table 2. This model obeys the modified Mohr–Coulomb yield criterion [35], which is defined as

$$f = -P \sin \varphi + \sqrt{J_2 K(\theta)^2 + A^2 \sin^2 \varphi} - c \cos \varphi = 0 \quad (1)$$

where:

$f$  = Yield surface

$P$  = Pressure, Pa

$\varphi$  = Angle of internal friction, °

$J_2$  = Second invariant of the stress deviator, Pa

$K(\theta)$  = Function of the angle in the deviatoric plane

$A$  = Drucker-Prager coefficient

$c$  = Cohesion, Pa

### 2.3.3. Meshing, Boundary, and Loading

Hypermesh was used to implement mesh generation. The upper surface of the blades were divided into quadrilateral meshes. The size of mesh was 8.5 mm. Then, regular hexahedral meshes were drawn along the contour line of the blades by line drag method, and the mesh size was 9.5 mm. Furthermore, the spiral blades and shafts were divided into tetrahedral meshes, and the size of mesh was 9.5 mm. The spiral cutters' element number was 64,093. The cuboid soil model was meshed by the map method. The size of mesh was 7 mm and the element number was 948,360. The finite element meshes of the soil were transformed into SPH particles. Except top face and the face where the spiral cutter begins to cut, all DOF of the soil's other faces were constrained. The rotational and forward velocity of the spiral cutter were the same as those measured in the field test.

### 2.3.4. Contact Definition

In the simulation model of the spiral cutter–soil system, the cutter is the FEM element and the soil is SPH particle. There is interaction between with the computational domains discretized by different methods at the interface. Therefore, it is necessary to define the interaction between them. The interaction algorithms on the interface mainly include Kinematic Constraint Method, Distributed Paramete Method and Penalty Method. Among them, penalty function method is widely used in numerical computation due to its symmetry and accurate conservation of momentum, etc. Therefore, this paper adopts penalty function method when dealing with the interaction between SPH and FEM [36]. When establishing the simulation model, the SPH node is defined as the slave node, and the FEM element surface on the interface in contact with the SPH node is defined as the master surface. SPH and FEM are coupled through the “nodes to surface” contact algorithm [33]. If the contact condition between SPH particles and the FEM element surface is satisfied, the contact force is determined via the penalty function method, and the force of SPH particles is applied to the FEM element surface, as shown in Figure 7. The left part is the calculation process of SPH. The right part is the FEM calculation process. Moreover, each blade and the spiral blade (including shaft) were set as a contact surface, respectively, for obtaining the forces acting on the different blades and the spiral blade (including shaft).

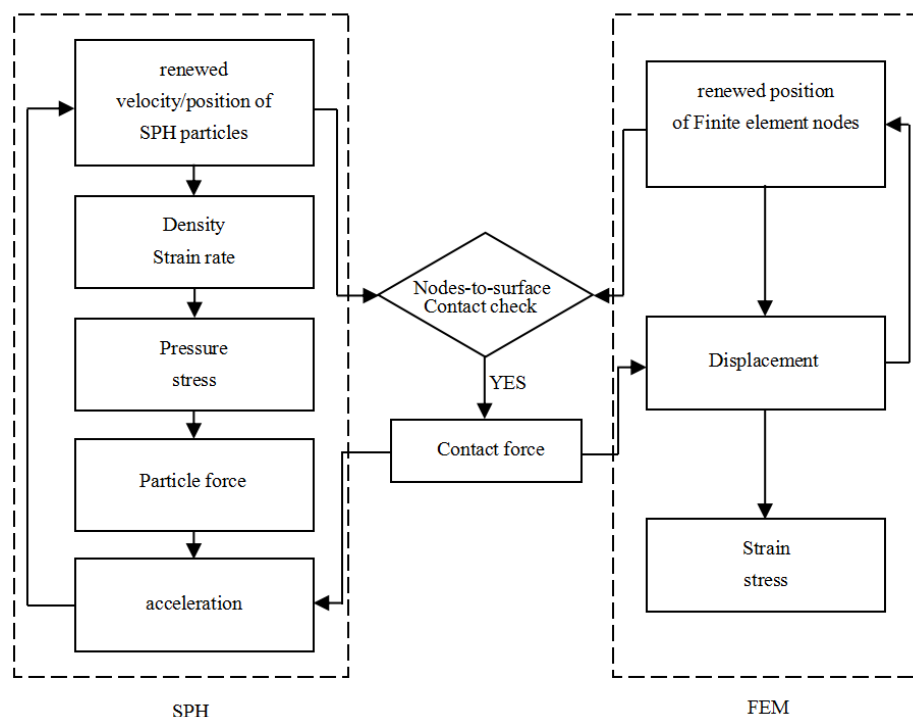


Figure 7. Flow chart of SPH-FEM contact algorithm.

2.4. Modeling Method Verification

The simulation test was conducted using the established model of the spiral cutter–soil system. We obtained the soil cutting torque curve of the spiral cutter in the middle stable stage of the simulation. Then, we compared this curve from the simulation with the one obtained from the field test to verify the reasonability of the modeling method for the spiral cutter–soil system.

2.5. Analysis of Working Mechanism

In the range of 30–50 cm tillage depth, the working resistance of the cutter varied with tillage depth, but the process of the cutter cutting the soil is the same. And the increase in tillage depth will lead to the increases of SPH particle number and calculation time significantly. Therefore, when analyzing the working mechanism of the spiral cutter, the thickness of the tillage layer was set to be the same as that of the verification model, which was also 30 cm.

Although there are fewer impurities in the soil of selected test site for torque measurement, which improves the verification accuracy of the rationality of the modeling method, the soil of the test site is not representative in Guangxi of China. Thus, for making the analysis more representative, this paper taken the red clay loam, which accounts for about 60% of the dry land in Guangxi, as the object, to carry on the simulation analysis of working mechanism. The soil samples were taken from a sugarcane field in Taiping Town, Wuming District, Nanning City, Guangxi Province, China (lat. 23.12° N, long. 108.39° E). The soil mechanical components are shown in Table 3. The measurement method of soil property parameters was the same as that in the literature [13]. The main property parameters of soil are shown in Table 4.

Table 3. Soil mechanical component in the analysis of work process.

Soil Particle Size/mm	2–1	1–0.5	0.5–0.25	0.25–0.075	0.075–0.02	0.02–0.002	<0.002
Mass percent (%)	6.24	8.96	11.33	11.15	16.28	28.65	17.39

**Table 4.** Soil main property parameters in the analysis of work process.

Depth/mm	Bulk Density /g·cm <sup>-3</sup>	Cohesion /Pa	Moisture Content /%	Internal Friction Angle /°	Elasticity Modulus /MPa	Bulk Modulus /MPa	Shear Modulus /MPa
0–100	1.256	37,434	23.53	29.78	8.7	7.25	3.346
100–200	1.266	31,701	27.37	22.45	5.5	4.583	2.115
200–300	1.385	41,470	26.67	26.31	7.0	5.833	2.692
300–400	1.371	44,128	28.70	25.32	6.5	5.417	2.5

When the spiral cutter cuts the soil, the separation process of the furrow slices in soil at different depths is different, and the breaking process of these furrow slices is also different. Hence, to facilitate the analysis of the working mechanism of spiral cutters, firstly, according to the observation of the separation and breaking simulation process, the separation and breaking mechanisms of the furrow slices of the upper-, middle- and lower-layer soil were analyzed, respectively. Then, the mechanism of soil cutting, crushing, uplifting and loosening, and the reasons of the larger topsoil clods and smaller lower clods after tillage were analyzed comprehensively. To observe each process in simulation clearly, except for the study object, the rest was hidden in LS-PrePost post-processor. When analyzing the separation of the furrow slices from the corresponding layer soil, only one spiral cutter and the corresponding layer soil which opposite the spiral cutter directly were shown. And when analyzing the breaking process of the furrow slices, only one furrow slice and two spiral cutters were shown.

In this paper, the cutting of separating furrow slices from soil was called separation cutting. When the cutting speed of the blade was greater than the moving speed of the furrow slice or the clod, the cutting of blade to the furrow slice or the clod was called velocity difference cutting. The cutting of the clod or the furrow slice with adjacent spiral cutter was called auxiliary cutting.

### 2.6. Analysis of Soil Cutting Force

For different depths of soil, the cutting resistance of the blades is different. Thus, firstly, the soil was divided into upper, middle and lower layers, and the forces of the blade cutting different soil layers were analyzed. Then, the forces of all working blades, spiral blade (including shaft) and spiral cutter were analyzed, respectively. Finally, according to these analyses, the reasons for the large cutting resistance and vibration of the spiral cutter were clarified.

## 3. Results and Discussion

### 3.1. Model Verification

In the verification test, the rotational and average forward velocity of the spiral cutter were 41.6 rad·s<sup>-1</sup> and 0.53 m·s<sup>-1</sup>, respectively. The soil-cutting torque curves in the stable stage of the test are shown in Figure 8. Figure 8a is the torque diagrams of the spiral cutter advancing 1 m in three field tests. Figure 8b is the torque diagram of the simulation test in the stable stage.

Figure 8 shows that the torque variation period of the simulation test is consistent with that of the three field areas, which is also 0.15 s. The average torque of simulation test is 474 N·m, and the average torque in the field tests is 482, 490, and 515 N·m, respectively. The torque of the simulation test is less than that of the physical test; we believe that this is the result of the complexity of the soil in the field and the simplification of the structure of the spiral cutter. And the torque relative errors of the simulation test and the field tests are 1.7%, 3.3%, and 8%, respectively, which shows that the modeling method of the spiral cutter–soil system is reasonable and the established model can be used for the working analysis of the spiral cutter.

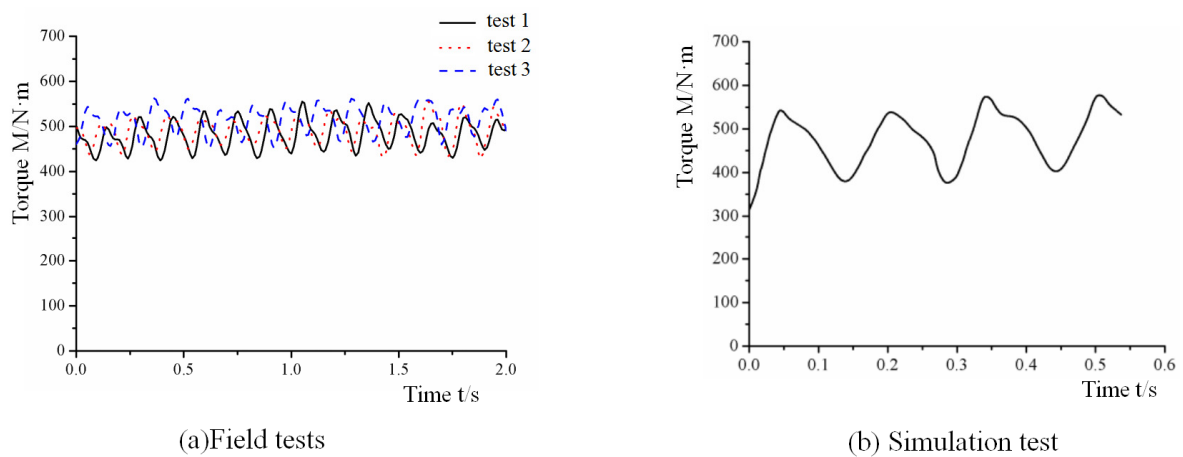


**Figure 8.** The soil cutting torque curves of spiral cutter.

### 3.2. Analysis of Working Mechanism

#### 3.2.1. Separation of Furrow Slice from Each Layer of Soil

##### (1) Separation in upper layer soil

When the spiral cutter cuts the soil at low forward and high rotating speed, the upper layer soil in front of the cutter first gradually lifts and bends under the forward pushing action of the cutter. Then, the lifted soil is cut by three adjacent blades from low to high in turn, and finally, the furrow slice is separated. Meanwhile, owing to cutting, bending, and extrusion, some broken soil is produced.

The upper part of the upper layer soil is unconstrained; hence, the uplifted height and length of the soil are larger, and the separated furrow slices are large. But Figure 9 shows that the uplifted height and length are different in each separating process. Thus, the volume of the separated furrow slice is different. The volume of the largest furrow slice is  $938.5 \text{ cm}^3$ . One of the separating processes is shown in Figure 10a.

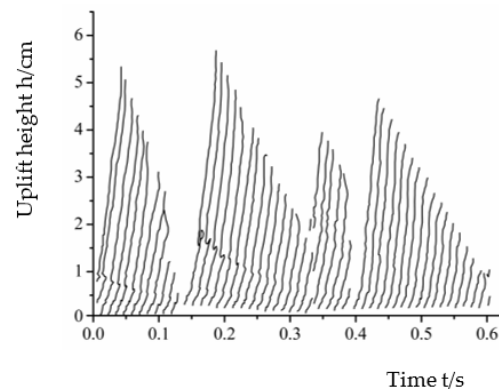


**Figure 9.** The movement trajectories of surface particles of the soil in front of the spiral cutter.

##### (2) Separation in middle-layer soil

The upper part of the middle layer soil is constrained by the upper-layer soil; thus, the maximum uplift height is small, about 1.7 cm. The separation of the furrow slices is mainly accomplished by three adjacent blades cutting from low to high in turn and the spiral blade cutting. The volume of the furrow slices is basically the same, but it is smaller than that of the largest furrow slice in the upper-layer soil, and more broken soil is produced. The volume of the largest furrow slice is  $438.6 \text{ cm}^3$ . One of the separating processes is shown in Figure 10b.

### (3) Separation in lower layer soil

The separation of the furrow slices is mainly accomplished by the spiral blade bottom edge and the blade cutting together. The bottom of the lower layer soil is cut by the bottom edge first, and then the side of the soil is cut by the blade to separate the furrow slice. In this process, a large number of broken soil is produced. The volume of the largest furrow slice is  $293 \text{ cm}^3$ , which is relatively minimal. One of the separating processes is shown in Figure 10c.

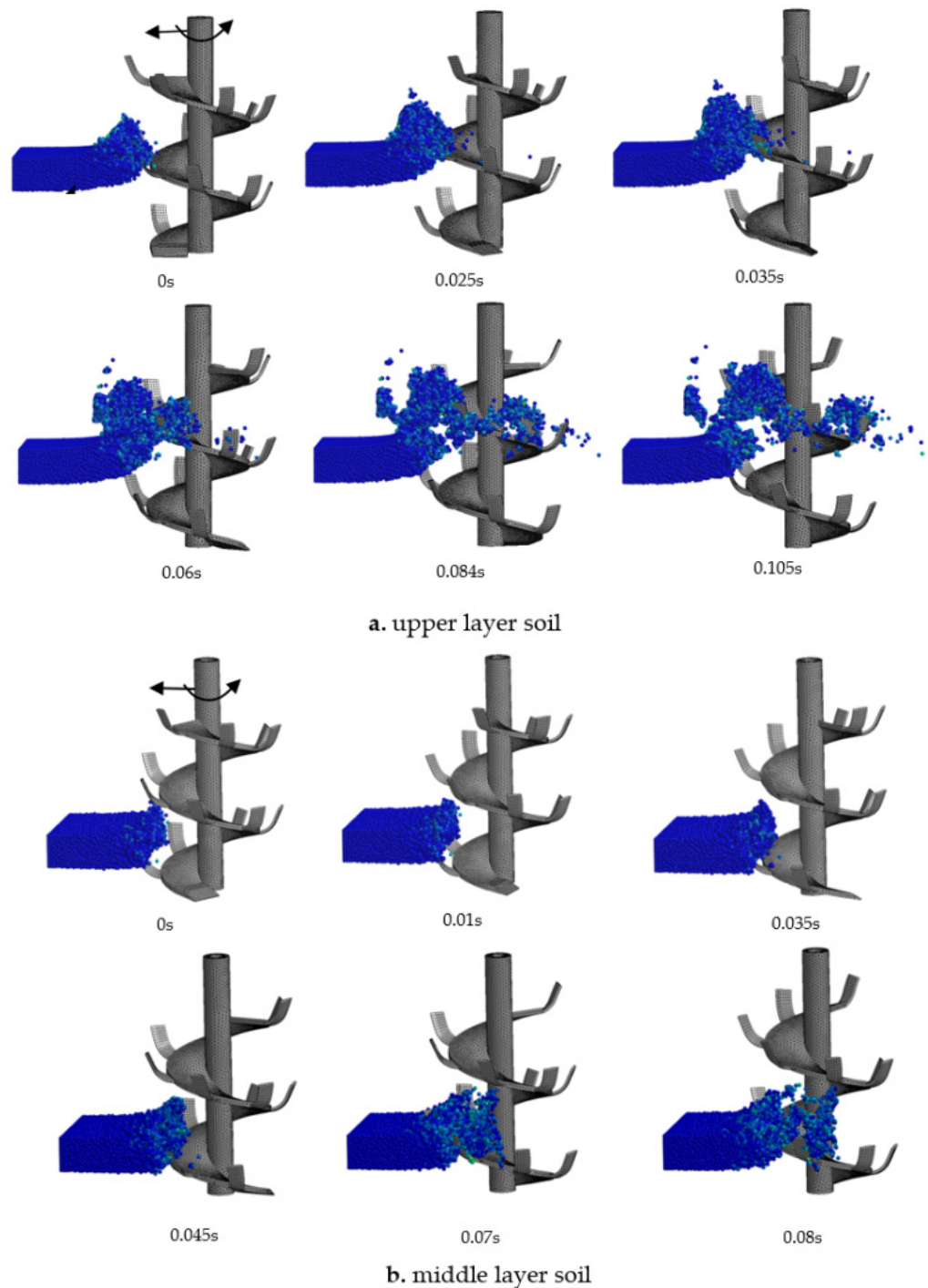
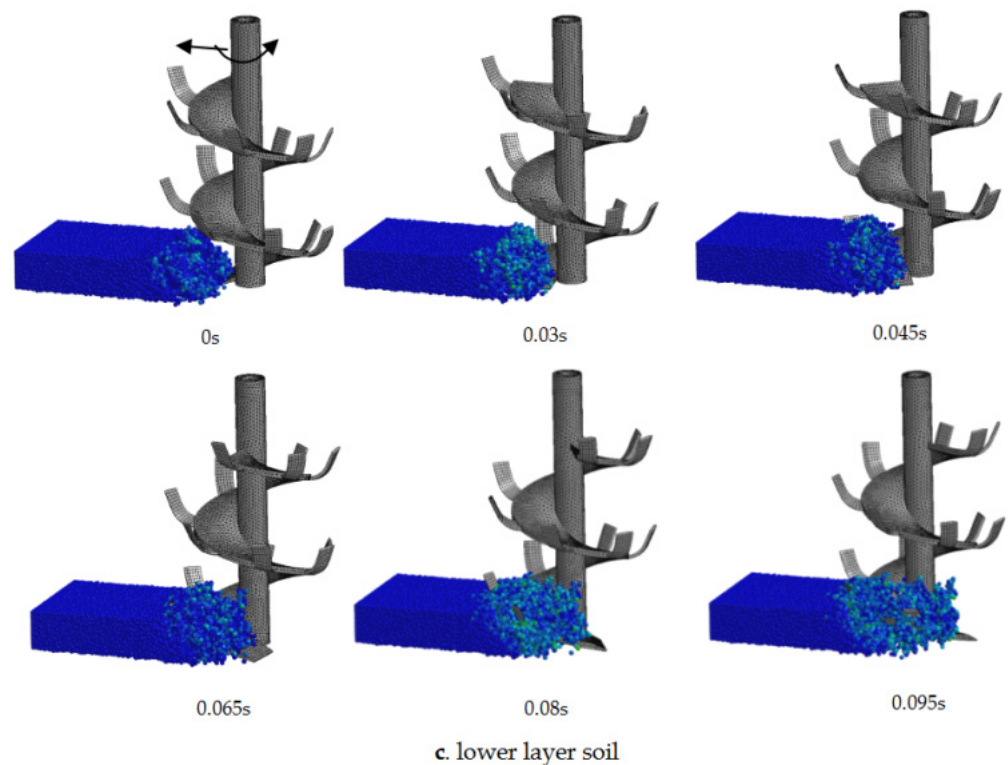


Figure 10. Cont.



**Figure 10.** Separation cutting process of the furrow slices.

### 3.2.2. Breaking of Furrow Slice

The separated furrow slices rotate and move upward under the action of the spiral cutter, meanwhile, move outward due to the centrifugal force. Moreover, the average cutting speed of the blades is  $8.11 \text{ m}\cdot\text{s}^{-1}$ , which is greater than the moving speed in the horizontal plane of the furrow slices. Hence, when the furrow slices contact with the blade edge, the velocity difference cutting occurs, and the furrow slices are broken into the clods. When the velocity difference cutting of the clods occurs, the clods would be further broken. Meanwhile, due to staggered setting of the blades of the two cutters, when the furrow slices or the clods make contact with the blade edge of the adjacent spiral cutter, the auxiliary cutting occurs, and the furrow slices or the clods are also broken. And these two kinds of cutting would continue until the clods leave the cutters.

The furrow slice and clod of the upper layer soil are both unconstrained; hence, they are prone to leave the cutters under the action of centrifugal force, resulting in insufficient cutting. Thus, after breaking the furrow slices, the volume of the larger clods are still relatively large. Figure 11a shows when breaking the largest furrow slice of the upper layer soil, the times of the velocity difference cutting and auxiliary cutting are both 2. After breaking, the median quality is 95.8 g.

The furrow slice and clod of the middle-layer soil are not prone to leave the cutters due to the constraint of the ambient soil and the upper-layer soil. The velocity difference cutting is relatively sufficient. Thus, after breaking, the larger clods are relatively small in volume. Figure 11b shows that when breaking the largest furrow slice of the middle-layer soil, the times of the velocity difference cutting and auxiliary cutting are 6 and 2, respectively. After breaking, the median quality is 11.1 g.

The furrow slice and clod of the lower layer soil are more difficult to leave the cutters due to the great constraint of the ambient soil and the middle-layer soil. The velocity difference cutting is sufficient. Therefore, after breaking, the larger clods are the smallest in volume. Figure 11c shows when breaking the largest furrow slice of the lower-layer soil, the times of the velocity difference cutting and auxiliary cutting are 9 and 1, respectively. After breaking, the median quality is 4.21 g.

Additionally, the velocities in the horizontal plane of the furrow slices and some of its clods in Figure 11 are shown in Figure 12, where the initial values of the curves are the velocities of the furrow slices, and the rest values are the velocities of some of its clods.

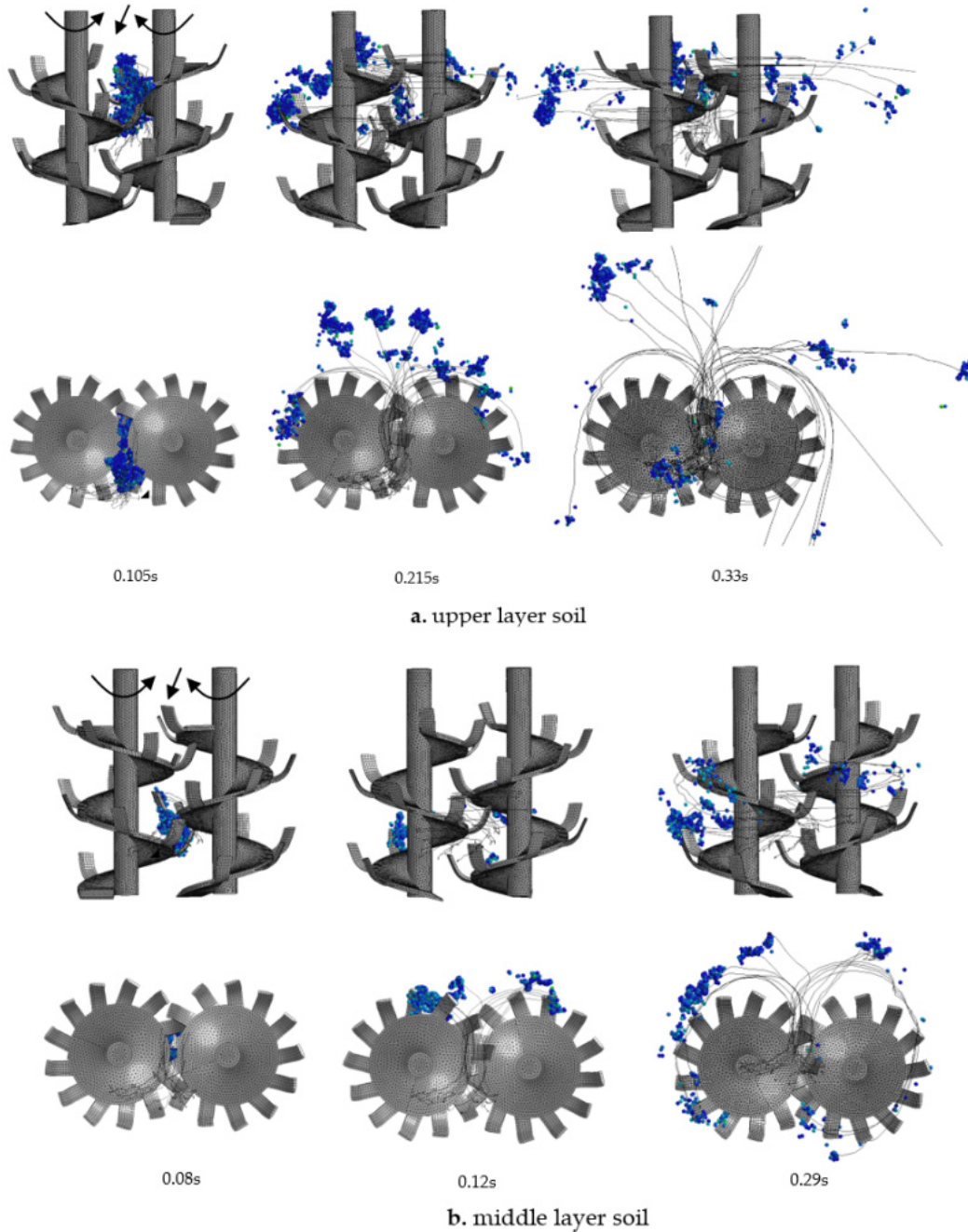
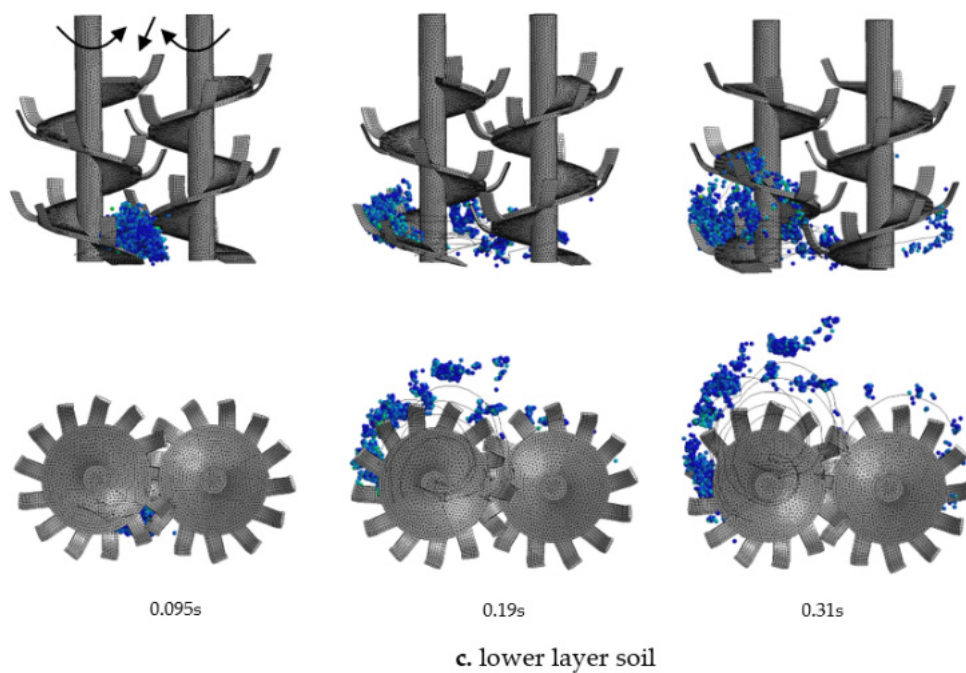
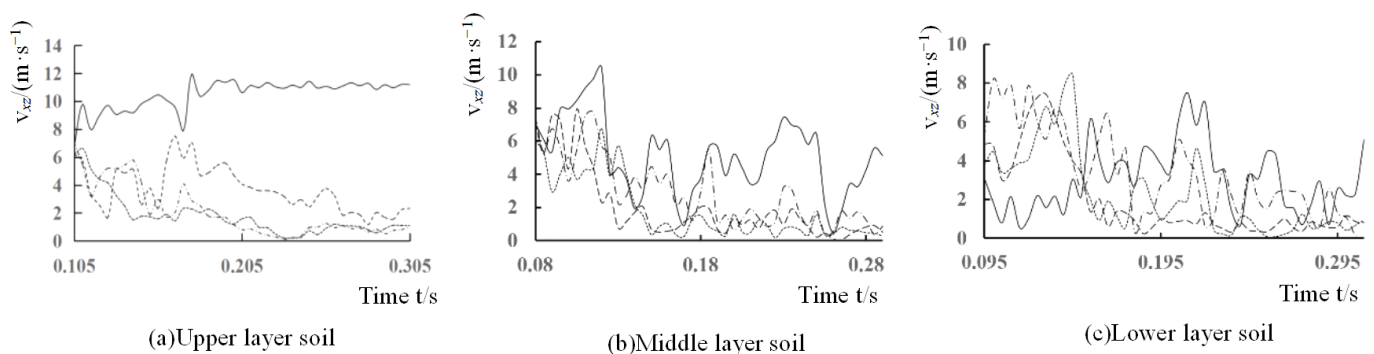


Figure 11. Cont.



**Figure 11.** Breaking process of the largest furrow slices.



**Figure 12.** Velocities of the largest furrow slices and some of its clods in the horizontal plane.

In the pictures of each layer soil, the main view is on the top and top view is on the bottom.

### 3.2.3. Working Mechanism of Spiral Cutters

The above analysis and the working simulation of the spiral cutters (Figure 13) show that when a pair of the spiral cutters rotate in reverse rapidly and move forward slowly, the blades and the spiral blades first cut the soil, and the furrow slices separate from the soil. Afterwards, these furrow slices rotate and move upward under the action of the spiral cutters and move outward under the action of centrifugal force. And during the movement, these furrow slices are cut into the clods via velocity difference cutting and auxiliary cutting. Then, when these clods continue to move in the spiral cutters, if the velocity difference cutting and the auxiliary cutting occur, the clods would be broken further. And as the clods of the upper-layer soil move upward, some of the clods fly away from the spiral cutters successively and then fall into the ground due to centrifugal force and gravity, and the rest of the clods, after the spiral cutters move to front of them, fall to the ground due to gravity. This is the main reason for the soil fragmentation, swelling and loosening. Gao et al. studied the working process of a vertical rotary tillage cutter with short blades installed on spiral blades. The soil fragmentation, swelling, and loosening of the cutter in this process are basically the same as that of the cutter in this paper. But because the

blade of this cutter is short, its auxiliary cutting effect is relatively small [37]. And the vertical spiral ditching device has a structure similar to that of the cutter in this article, so its soil lifting and throwing movement process is similar to that of the cutter in this article. However, due to the lack of blades and there being only a single axis of the device, there is no separation cutting, velocity difference cutting, and auxiliary cutting in the cutting and crushing processes [38]. In addition, because the blade roller of the horizontal rotary tiller is placed horizontally, the soil breaking process of the cutter in this paper is different from that of the horizontal rotary tiller.

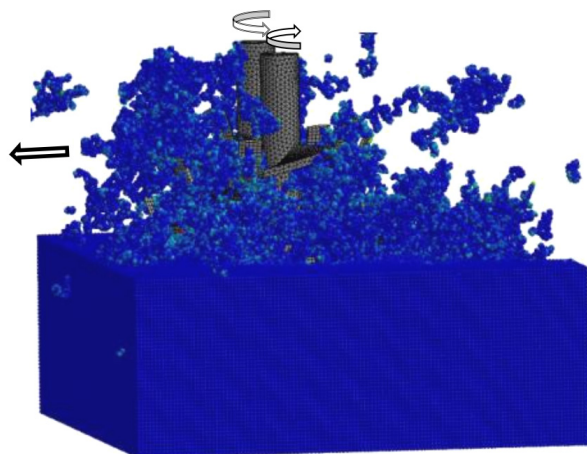


**Figure 13.** Working simulation of spiral cutters.

Due to the larger volume of the furrow slice of the upper layer soil, some of the clods formed by the initial velocity difference cutting and auxiliary cutting are large in volume. Moreover, there is no constraint on the top of these large volume clods. These clods are prone to leave the spiral cutters due to the centrifugal force, which leads to insufficient velocity difference cutting and auxiliary cutting. Thus, there are a lot of the larger volume clods in the top soil layer and the soil breaking degree is low after tillage. In contrast, the outward and upward movement of the larger volume clods of the middle-layer soil is constrained by the ambient soil and the upper-layer soil. This constraint prevents these clods from easily leaving the spiral cutters, leading to a relatively sufficient velocity difference cutting. Consequently, the larger volume clods in the middle-layer soil are relatively smaller after tillage. The outward and upward movements of the large volume clods of the lower layer soil are constrained greatly by the surrounding soil and the middle-layer soil. Consequently, the clods are difficult to remove from the spiral cutters, which brings about sufficient velocity difference cutting. Hence, the larger volume clods in the lower-layer soil are the smallest after tillage. This is the reason of the larger topsoil clods and smaller lower clods after tillage. Therefore, the structure of the spiral cutter above the ground requires further optimization to improve the breaking degree of the surface layer soil.

### 3.3. Analysis of Soil Cutting Force

#### 3.3.1. Single Blade Force

A schematic diagram of a single blade cutting soil is shown in Figure 14.  $y$  direction of the coordinate system is going from the inside out in Figure 14.  $\theta$  is the angle of blade rotation. Force of single blade is shown in Figure 15. It can be seen from Figures 14 and 15 that when the blade cuts the upper, middle and lower layer soil, with the increase of  $\theta$ , the change of forces in different directions of the blade and resultant force of the blade are basically the same; however, the maximum values of these forces are different. The upper part of the upper-layer soil is unconstrained, the middle layer soil is constrained to some extent, and the lower layer soil is constrained greatly; thus the blade forces cutting the lower-layer soil are the largest, those of the middle-layer soil are the second, and the those

of the upper-layer soil are the smallest. The  $(f_r)_{\max}$  of the upper-, middle-, and lower-layer soil is 453.3 N, 552.5 N, and 680.9 N, respectively. And the average value of  $(f_x)_{\max}$ ,  $(f_z)_{\max}$ ,  $(f_y)_{\max}$  and  $(f_r)_{\max}$  of three soil layers is 516.9 N, 435.9 N, 186.2 N, and 562.2 N, respectively. And the soil cutting resistance of the blade of the horizontal rotary tiller is much smaller than that of the blade in this paper because its blade roller is placed horizontally [39].

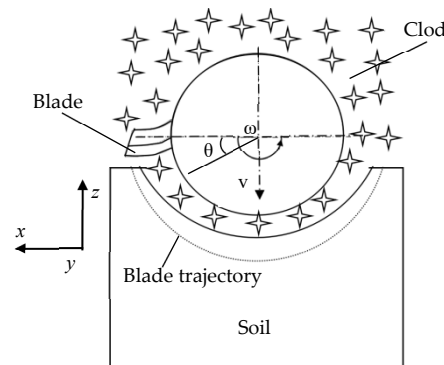


Figure 14. Schematic diagram of single blade cutting soil.

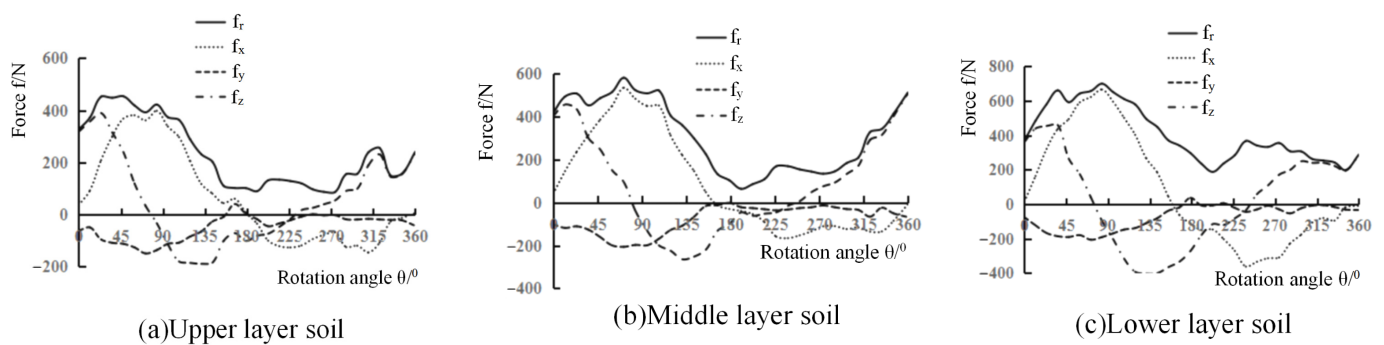


Figure 15. Force of single blade.  $f_r$ : resultant force,  $f_x$ : horizontal force,  $f_y$ : vertical force,  $f_z$ : force in the forward direction.

### 3.3.2. The Force of All Working Blades

Forces on the spiral cutter's blades are shown in Figure 16a. When the spiral cutter rotates and cuts the soil for one cycle,  $F_{1x}$ ,  $F_{1z}$ , and  $F_{1r}$  increase first and then decrease, while  $F_{1y}$  increases first and then decreases (negative) with slow changes. The maximum values of  $F_{1x}$ ,  $F_{1z}$ ,  $F_{1y}$  and  $F_{1r}$  are 2669.7, 1591, 1163, and 2979.5 N, respectively, and the minimum values are 38.5, 13.46, 157.7, and 556.7 N, respectively. These forces change periodically in the cutting process, and the change period is 0.15 s.

When the spiral cutter rotates and cuts the soil for one cycle, the number of blades simultaneously cutting the soil changes due to the asymmetric distribution of the blades on the cross section of the spiral cutter; thus,  $F_{1x}$ ,  $F_{1z}$ ,  $F_{1y}$  and  $F_{1r}$  increase first and then decrease. And when the number of the blades cutting the soil simultaneously is two,  $F_{1x}$ ,  $F_{1z}$ ,  $F_{1y}$  and  $F_{1r}$  are the smallest and their values are 38.5, 13.46, 157.7, and 556.7 N, respectively, and when the number of the blades cutting the soil simultaneously is four, these forces are the largest and their values are 2669.7, 1591, 1163, and 2979.5 N, respectively, which indicates that the number of the blades cutting the soil simultaneously has a great influence on the forces change of the spiral cutter's blades. The force of the spiral cutter's blades is large when the number of the blades cutting the soil simultaneously is too many.

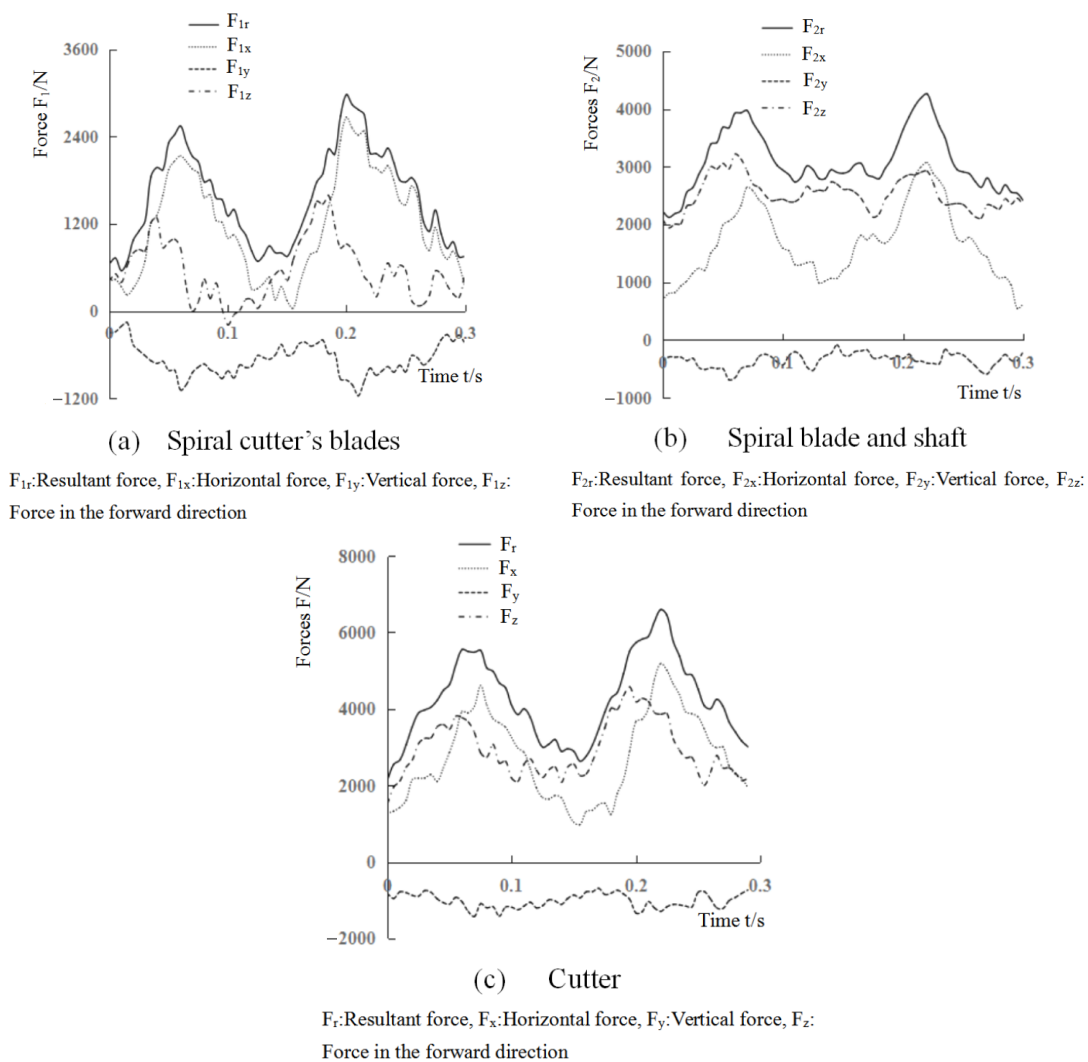


Figure 16. Forces on different components.

### 3.3.3. Forces on Spiral Blade and Shaft

Forces on spiral blade and shaft are shown in Figure 16b. When the spiral cutter rotates and cuts the soil for one cycle,  $F_{2x}$ ,  $F_{2z}$  and  $F_{2r}$  increase first and then decrease, while the change of  $F_{2y}$  is small (negative). The maximum value of  $F_{2x}$ ,  $F_{2z}$  and  $F_{2r}$  are 2861, 3073.3, and 4119.7 N, respectively, and the minimum values are 755.3, 2061.2, and 2246.2 N, respectively. The change period of these forces is also 0.15 s.

When the spiral cutter rotates and cuts the soil for one cycle, because of the asymmetric distribution of the spiral teeth of the spiral blade on the cross section of the spiral cutter, the number of the spiral teeth cutting the soil simultaneously and the position where the soil is cut by the spiral teeth are both different. Therefore,  $F_{2x}$ ,  $F_{2z}$ , and  $F_{2r}$  first increase and then decrease. When one spiral tooth is cutting the upper layer soil and the bottom edge of the spiral blade is cutting the lower layer soil, meanwhile, when the spiral tooth and the bottom edge are both facing the forward direction,  $F_{2x}$ ,  $F_{2z}$  and  $F_{2r}$  are the largest. When one spiral tooth is cutting the middle layer soil and facing the forward direction,  $F_{2x}$ ,  $F_{2z}$ , and  $F_{2r}$  are the smallest.  $(F_{2x})_{max}$  is 2861 N, and  $(F_{2x})_{min}$  is 755.3 N. Moreover, the cutting resistance of cutting upper layer soil is smaller than  $(F_{2x})_{min}$ , which indicates that the cutting resistance of the bottom edge of the spiral blade is larger. The maximum and minimum value of  $F_{2z}$  are 3073.3 N and 2061.2 N, respectively, and their difference is relatively small, which indicates that the number of the spiral teeth cutting the soil simultaneously has a relatively small influence on  $F_{2z}$ .

### 3.3.4. Forces on Spiral Cutter

Forces on cutter are shown in Figure 16c. When the spiral cutter rotates and cuts the soil for one cycle,  $F_x$ ,  $F_z$ , and  $F_r$  increase first and then decrease, while  $F_y$  changes slowly (negative) and its value is relatively small. The maximum value of  $F_x$ ,  $F_z$  and  $F_r$  are 4901, 4192 and 6075 N, respectively. And the minimum values are 978.5, 1518.7, and 2148.1 N, respectively. The change period of these forces is also 0.15 s. The amplitude of  $F_r$  is 1963.5 N.

The force of the spiral cutter is the resultant force of the forces of the blades and the spiral blade (including shaft). Thus, the change of  $F_x$ ,  $F_z$ ,  $F_y$ , and  $F_r$  is basically the same as that of the forces of the blades and the spiral blade (including shaft). Figures 16c and 17 illustrate that when the spiral tooth and the bottom edge of the spiral blade cut the upper and the lower layer soil respectively, and four blades cut the soil simultaneously,  $F_x$ ,  $F_z$ , and  $F_r$  are the largest. When one spiral tooth cuts the middle-layer soil and two blades cut the soil simultaneously,  $F_x$ ,  $F_z$  and  $F_r$  are the smallest. Furthermore,  $(F_x)_{\max}$ ,  $(F_z)_{\max}$ , and  $(F_r)_{\max}$  are 4901, 4192, and 6075 N, respectively, which indicates that the maximum forces of the spiral cutter are large. And the reason is that the cutting resistance of the blade and the spiral blade's bottom edge are larger, and the number of the blades cutting the soil simultaneously is too many. Moreover, the amplitude of  $F_r$  is 1963.5 N, and its frequency is 6.7 Hz. However, the modal analysis of the spiral cutter shows that its lowest natural frequency was 52 Hz. This shows that the large amplitude of the exciting force, which is caused by the asymmetry of the cross section of the spiral cutter, is the reason for the large vibration of the spiral cutter. Therefore, optimizing the structure of the blade and the bottom edge of the spiral blade and reducing the number of the blades cutting the soil simultaneously can effectively reduce the cutting resistance of the spiral cutter, and reducing the asymmetric design of the cross section of the spiral cutter can effectively reduce the vibration of the spiral cutter.

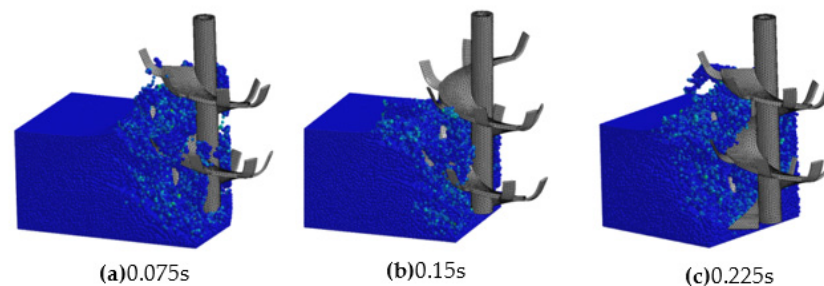


Figure 17. Simulation screenshot of the spiral cutter rotates and cuts the soil for one cycle.

## 4. Conclusions

In this paper, the rationality of the modeling method of soil–spiral cutter system based on SPH method has been verified with the field test. Furthermore, the working mechanism and force of the spiral cutter have been investigated using the established system model. The following major conclusions have been obtained:

- In the DVRT, the soil fragmentation, swelling, and loosening are mainly the comprehensive results of the separation cutting, velocity difference cutting, auxiliary cutting, and spiral blade's lifting effect on the soil. The reason for the larger topsoil clods after tillage is that the furrow slices of topsoil are larger, and the velocity difference cutting of the furrow slices is not enough.
- The cutting resistance of the single blade and the bottom edge of the spiral blade are larger. The number of the blades cutting the soil simultaneously has a great influence on the forces of the spiral cutter's blades.
- The cutting resistance of the blade and the spiral blade's bottom edge is larger, and the number of the blades cutting the soil simultaneously is too many, which is the reason for the large cutting resistance of the spiral cutter. The asymmetric of the spiral cutter cross section leads to larger change in the spiral cutter forces. The amplitude

of the exciting force of the spiral cutter reaches 1963.5 N, which is the reason for its large vibration.

- (d) It is suggested that the symmetrical double spiral blade's spiral cutter should be used, the blade distribution should be set reasonably, and the structure of the spiral cutter above the ground, blade and spiral blade's bottom edge should be optimized. These improvements should improve the breaking degree of topsoil after tillage, and reduce the cutting resistance and vibration of the spiral cutter.
- (e) This study's contribution lies in its comprehensive analysis of factors affecting spiral cutter–soil interaction, leading to insights into soil fragmentation, clod formation, cutting resistance, and vibration. These research findings have great guiding significance for the optimization of the existing cutter and the innovative design of the new cutter, and the research methods of the paper can be used for reference in the research of related tillage components.

**Author Contributions:** Conceptualization, W.Y.; Methodology, W.Y.; Software, X.X.; Validation, R.P. and S.G.; Writing—Original Draft Preparation, W.Y.; Writing—Review and Editing, W.Y.; Project Administration, J.Y. All authors have read and agreed to the published version of the manuscript.

**Funding:** This work was supported by grants from the National Natural Science Foundation of China (Grant Nos 32160422 and 51565003), Guangxi Natural Science Foundation (Grant No. 2023GXNS-FAA026376).

**Institutional Review Board Statement:** Not applicable.

**Informed Consent Statement:** Not applicable.

**Data Availability Statement:** The data that support the findings of this study are available from the corresponding author upon reasonable request.

**Conflicts of Interest:** The authors declare no conflict of interest.

## References

1. Florian, S.; Axel, D.; Inga, H.; Oliver, S.; Sabine, J.S. The effect of deep tillage on crop yield—What do we really know? *Soil Tillage Res.* **2017**, *174*, 193–204. [[CrossRef](#)]
2. Zhang, X.C.; Guo, J.; Ma, Y.F.; Yu, X.F.; Hou, H.Z.; Wang, H.L.; Fang, Y.J.; Tang, Y.F. Effects of vertical rotary subsoiling with plastic mulching on soil water availability and potato yield on a semiarid Loess plateau, China. *Soil Tillage Res.* **2020**, *199*, 104591. [[CrossRef](#)]
3. Yao, R.J.; Gao, Q.C.; Liu, Y.X.; Li, H.Q.; Yang, J.S.; Bai, Y.C.; Zhu, H.; Wang, X.P.; Xie, W.P.; Zhang, X. Deep vertical rotary tillage mitigates salinization hazards and shifts microbial community structure in salt-affected anthropogenic-alluvial soil. *Soil Tillage Res.* **2023**, *227*, 105627. [[CrossRef](#)]
4. Yin, J.D.; Zhang, X.C.; Ma, Y.F.; Yu, X.F.; Hou, H.Z.; Wang, H.L.; Fang, Y.J. Vertical rotary sub-soiling under ridge–furrow with plastic mulching system increased crops yield by efficient use of deep soil moisture and rainfall. *Agric. Water Manag.* **2022**, *271*, 107767. [[CrossRef](#)]
5. Zhang, X.C.; Ma, Y.F.; Yu, X.F.; Hou, H.Z.; Wang, H.L.; Fang, Y.J. Vertical rotary sub-soiling affects soil moisture characteristics and potato water utilization. *Agron. J.* **2021**, *113*, 657–669. [[CrossRef](#)]
6. Yang, J.J.; Tan, W.J.; Han, J.R.; Li, F.M.; Zhang, F. Distribution pattern of rainwater in soil under vertical deep rotary tillage in dryland farmland. *Agric. Water Manag.* **2022**, *273*, 107891. [[CrossRef](#)]
7. Wei, B.H.; Li, S.W.; Gan, X.Q.; Wei, Y.B.; Li, L.P. Rotary Cutting Type Deep Tillage Powder Ridge Multifunctional Machine. China Patent 201010270614.3, 26 December 2012.
8. Li, S.W. A Powder Ridge Machine for Sowing and Its Sowing Method. China Patent 201510285383.6, 21 September 2016.
9. Liu, J.B.; Qiao, J.F.; Zhu, W.H.; Gu, L.M.; Dai, S.T.; Zhang, M.W.; Huang, L.; Wang, J.Z.; Guo, G.J. Powder Ridge Drill and Powder Ridge Machine. China Patent 201621059688.1, 22 March 2017.
10. Li, G.D. Brief discussion on the strength and lubrication of the driving box of rotary cutting tool of loose tillage powder ridge machine. *Agric. Mech. Guangxi* **2015**, *5*, 26–27. (In Chinese) [[CrossRef](#)]
11. Bentaher, H.; Ibrahmi, A.; Hamza, E.; Hbaieb, M.; Kantchev, G.; Maalej, A.; Arnold, W. Finite element simulation of moldboard–soil interaction. *Soil Tillage Res.* **2013**, *134*, 11–16. [[CrossRef](#)]
12. Li, M.; Xu, S.; Yang, Y.W.; Guo, L.; Tong, J. A 3D simulation model of corn stubble cutting using finite element method. *Soil Tillage Res.* **2017**, *166*, 43–51. [[CrossRef](#)]
13. Tagar, A.A.; Ji, C.Y.; Adamowski, J.; Malard, J.; Chen, S.Q.; Ding, Q.S.; Abbasi, N.A. Finite element simulation of soil failure patterns under soil bin and field testing conditions. *Soil Tillage Res.* **2015**, *145*, 157–170. [[CrossRef](#)]

14. Hadi, A.N.; Seyed, H.K.; Mojtaba, N.B.; Hossein, R.K. Combined finite element and statistical models for predicting force components on a cylindrical mouldboard plough. *Biosyst. Eng.* **2019**, *186*, 168–181. [[CrossRef](#)]
15. Upadhyay, G.; Raheman, H.; Rasool, S. Three dimensional modelling and stress analysis of a powered single acting disc harrow using FEA. *Curr. Agric. Res.* **2017**, *5*, 203–219. [[CrossRef](#)]
16. Wang, Y.; Zhang, D.; Yang, L.; Cui, T.; Jing, H.; Zhong, X. Modeling the interaction of soil and a vibrating subsoiler using the discrete element method. *Comput. Electron. Agric.* **2020**, *174*, 105518. [[CrossRef](#)]
17. Chen, Y.; Munkholm, L.J.; Nyord, T. A discrete element model for soil–sweep interaction in three different soils. *Soil Tillage Res.* **2013**, *126*, 34–41. [[CrossRef](#)]
18. Tekeste, M.Z.; Balvanz, L.R.; Hatfield, J.L.; Ghorbani, S. Discrete element modeling of cultivator sweep-to-soil interaction: Worn and hardened edges effects on soil-tool forces and soil flow. *J. Terramech.* **2019**, *82*, 1–11. [[CrossRef](#)]
19. Ucgul, M.; Saunders, C.; Fielke, J.M. Discrete element modelling of tillage forces and soil movement of a one-third scale mouldboard plough. *Biosyst. Eng.* **2017**, *155*, 44–54. [[CrossRef](#)]
20. Wang, X.Z.; Zhang, Q.K.; Huang, Y.X.; Ji, J.T. An efficient method for determining DEM parameters of a loose cohesive soil modelled using hysteretic spring and linear cohesion contact models. *Biosyst. Eng.* **2022**, *215*, 283–294. [[CrossRef](#)]
21. Ibrahmi, A.; Bentaher, H.; Hbaieb, M.; Maalej, A.; Mouazen, A.M. Study the effect of tool geometry and operational conditions on mouldboard plough forces and energy requirement: Part 1. Finite element simulation. *Comput. Electron. Agric.* **2015**, *117*, 258–267. [[CrossRef](#)]
22. Abo, A.A.; Kharmanda, M.G.; Hami, A.E.; Mouazen, A.M. Estimating the variability of tillage forces on a chisel plough shank by modeling the variability of tillage system parameters. *Comput. Electron. Agric.* **2011**, *78*, 61–70. [[CrossRef](#)]
23. Dun, G.Q.; Chen, H.T.; Li, A.; Feng, Y.N.; Yang, J.L.; Ji, W.Y. Effect of rotation direction of knife teeth configuration on clearing straw unit performance for no-tillage and straw mulching precision seeder. *Trans. CSAE* **2015**, *31*, 48–56. (In Chinese) [[CrossRef](#)]
24. Gao, J.M.; Liu, X.D.; Qi, H.D.; Lakhiar, I.A. Simulation and experiment of soil casting during oblique submerged reversely rotary tillage. *Trans. CSAE* **2019**, *35*, 54–63. (In Chinese) [[CrossRef](#)]
25. Han, Y.J.; Li, Y.W.; Zhao, H.H.; Chen, H.; Liu, D.X. Simulation of soil cutting by vertical rotary blade based on SPH method. *J. Southwest Univ. (Nat. Sci. Ed.)* **2016**, *38*, 150–155. (In Chinese) [[CrossRef](#)]
26. Kang, J.M.; Li, S.J.; Yang, X.J.; Liu, L.J.; Li, C.R. Experimental verification and simulation analysis on power consumption of disc type ditcher. *Trans. CSAE* **2016**, *32*, 8–15. (In Chinese) [[CrossRef](#)]
27. Lu, C.Y.; He, J.; Li, H.W.; Wang, Q.J.; Zheng, Z.Q.; Zhang, X.C. Simulation of soil cutting process by plane blade based on SPH method. *Trans. CSAM* **2014**, *45*, 134–139. (In Chinese) [[CrossRef](#)]
28. Li, S.T.; Chen, X.B.; Chen, W.; Zhu, S.P.; Li, Y.W.; Yang, L.; Xie, S.Y.; Yang, M.J. Soil-cutting simulation and parameter optimization of handheld tiller's rotary blade by Smoothed Particle Hydrodynamics modelling and Taguchi method. *J. Clean. Prod.* **2018**, *179*, 55–62. [[CrossRef](#)]
29. Li, Y.W.; Zhang, G.Y.; Zhang, Z.; Zhang, Y.; Hu, T.D.; Cao, Q.Q. Development of low power-consumption multi-helical rotavator for small vertical-shaft deep-cultivator. *Trans. CSAE* **2019**, *35*, 72–80. (In Chinese) [[CrossRef](#)]
30. Lin, Y.L.; Yang, L.; Liu, S.R.; Zhao, X.Y.; Cao, C.; Li, C.L. Virtual simulation technology based research on subsoiling process. *Proc. Inst. Mech. Eng. Part C J. Mech. Eng. Sci.* **2019**, *233*, 1493–1503. [[CrossRef](#)]
31. Yang, W.; Yang, J.; Jia, F.Y.; Wang, Q.Y.; Huang, Y.Q. Numerical simulation of digging operation of cassava root planted in red clay. *J. Mech. Eng.* **2013**, *49*, 135–143. (In Chinese) [[CrossRef](#)]
32. Li, Y.M.; Ye, X.F.; Xu, L.Z.; Pang, J.; Ma, Z. Construction and performance experiment of load test system for half axle of combine harvester. *Trans. CSAE* **2013**, *29*, 35–41. (In Chinese) [[CrossRef](#)]
33. LSTC. *LS-DYNA v8.0 Keyword User's Manual*; Livermore Software Technology Corporation: Livermore, CA, USA, 2016.
34. Lewis, B.A. *Manual for LS-DYNA Soil Material Model 147*; Department of Transportation, Federal Highway Administration: Washington, DC, USA, 2004.
35. Abbo, A.J.; Sloan, S.W. A smooth hyperbolic approximation to the Mohr-Coulomb yield criterion. *Comput. Struct.* **1995**, *54*, 427–441. [[CrossRef](#)]
36. Hallquist, J.O. *LS-DYNA Theory Manual*; Livermore Software Technology Corporation: Livermore, CA, USA, 2006.
37. Gao, J.; Shen, Y.; Ma, B. Optimized design of touching parts of soil disinfection machine based on strain sensing and discrete element simulation. *Sensors* **2023**, *23*, 6369. [[CrossRef](#)]
38. Gao, W.Y.; Lin, J.; Li, B.F.; Ma, T. Parameter optimization and experiment for spiral type opener device of maize straw deep bury and returning machine. *Trans. CSAM* **2018**, *49*, 45–54. (In Chinese) [[CrossRef](#)]
39. Fang, H.M.; Ji, C.Y.; Zhang, Q.Y.; Guo, J. Force analysis of rotary blade based on distinct element method. *Trans. CSAE* **2016**, *32*, 54–59. (In Chinese) [[CrossRef](#)]

**Disclaimer/Publisher's Note:** The statements, opinions and data contained in all publications are solely those of the individual author(s) and contributor(s) and not of MDPI and/or the editor(s). MDPI and/or the editor(s) disclaim responsibility for any injury to people or property resulting from any ideas, methods, instructions or products referred to in the content.